MicroRNA-146a Mimics Reduce the Peripheral Neuropathy in Type 2 Diabetic Mice

Xian Shuang Liu,[1] Baoyan Fan,[1] Alexandra Szalad,[1] Longfei Jia,[1] Lei Wang,[1] Xinli Wang,[1] Wanlong Pan,[1,2] Li Zhang,[1] Ruilan Zhang,[1] Jiani Hu,[3] Xiao Ming Zhang,[4] Michael Chopp,[1,5] and Zheng Gang Zhang[1]

Diabetes 2017;66:3111–3121 | https://doi.org/10.2337/db16-1182

MicroRNA-146a (miR-146a) regulates multiple immune diseases. However, the role of miR-146a in diabetic peripheral neuropathy (DPN) has not been investigated. We found that mice (*db/db*) with type 2 diabetes exhibited substantial downregulation of miR-146a in sciatic nerve tissue. Systemic administration of miR-146a mimics to diabetic mice elevated miR-146a levels in plasma and sciatic nerve tissue and substantially increased motor and sensory nerve conduction velocities by 29 and 11%, respectively, and regional blood flow by 50% in sciatic nerve tissue. Treatment with miR-146a mimics also considerably decreased the response in *db/db* mice to thermal stimuli thresholds. Histopathological analysis showed that miR-146a mimics markedly augmented the density of fluorescein isothiocyanate–dextran-perfused blood vessels and increased the number of intraepidermal nerve fibers, myelin thickness, and axonal diameters of sciatic nerves. In addition, miR-146a treatment reduced and increased classically and alternatively activated macrophage phenotype markers, respectively. Analysis of miRNA target array revealed that miR-146a mimics greatly suppressed expression of many proinflammatory genes and downstream related cytokines. Collectively, our data indicate that treatment of diabetic mice with miR-146a mimics robustly reduces DPN and that suppression of hyperglycemia-induced proinflammatory genes by miR-146a mimics may underlie its therapeutic effect.

More than two-thirds of patients with diabetes develop neuropathy. There is currently no effective treatment for diabetic peripheral neuropathy (DPN) (1). The development and progression of diabetic neuropathy correlates closely with marked neurovascular abnormalities (2). Vascular dysfunction induced by diabetes starts very early and precedes the appearance of nerve conduction velocity deficits (2,3). Damaged microvasculature supplying the peripheral nerves leads to impairment of the nerve fibers and eventually to symptoms of painful diabetic neuropathy, including loss of sensation and foot ulceration (2,4). Therapies targeting neurovascular function have been demonstrated to improve nerve function in experimental DPN (5–7).

Experimental and clinical studies demonstrate that inflammation, especially proinflammatory cytokine (tumor necrosis factor-α [TNF-α], interleukin [IL]-1β, IL-6, and IL-8) and chemokine (MCP-1) production, is associated with microvascular complications of diabetes, including neuropathy (8,9). Among them, TNF-α and IL-6 cytokines are highly related to DPN. Patients with DPN have increased TNF-α and IL-6 levels in the plasma, and rodents with DPN induced by streptozotocin show increased levels of these two cytokines in the sciatic nerves (8–10). In addition, TNF-α–deficient diabetic mice fail to develop changes in nociceptive behavior and nerve conduction velocity (11), whereas administration of TNF-α into the sciatic nerve induces a reduction in motor nerve conduction velocity (8–10). Thus, the interruption or blockade of proinflammatory signaling pathways may provide important therapeutic targets and potentially reverse the deleterious effects of proinflammatory factors on neurovascular function, thereby preventing the progression of DPN.

MicroRNAs (miRNAs) are small noncoding RNAs emerging as key regulators in the pathogenesis of hyperglycemia-induced

[1]Department of Neurology, Henry Ford Health System, Detroit, MI
[2]Sichuan Key Laboratory of Medical Imaging and Department of Microbiology and Immunology, North Sichuan Medical College, Nanchong, Sichuan, China
[3]Department of Radiology, Wayne State University, Detroit, MI
[4]Sichuan Key Laboratory of Medical Imaging and Department of Radiology, Affiliated Hospital of North Sichuan Medical College, Nanchong, Sichuan, China
[5]Department of Physics, Oakland University, Rochester, MI

Corresponding author: Xian Shuang Liu, xsliu@neuro.hfh.edu.

Received 3 October 2016 and accepted 2 September 2017.

This article contains Supplementary Data online at http://diabetes.diabetesjournals.org/lookup/suppl/doi:10.2337/db16-1182/-/DC1.

vascular damage (12). miR-146a is one of the best characterized miRNAs in the regulation of innate and adaptive immunity and inflammatory diseases (13). miR-146a is involved in developing diabetic retinopathy and diabetic wound healing (14,15). Patients with diabetes with single nucleotide polymorphisms of miR-146a have increased susceptibility to diabetic microvascular complications, including diabetic neuropathy, retinopathy, and nephropathy (16–18). However, whether miR-146a has a therapeutic effect on DPN remains unknown. Using a highly clinically relevant mouse model of type 2 diabetes that develops severe peripheral neuropathy (19), we found that treatment of diabetic mice with miR-146a mimics robustly increased regional blood flow in sciatic nerves and reduced DPN.

RESEARCH DESIGN AND METHODS

Animals

All experimental procedures were carried out in accordance with the National Institutes of Health Guide for the Care and Use of Laboratory Animals and approved by the institutional Animal Care and Use Committee of Henry Ford Hospital. Male BKS.Cg-$m^{+/+}Lepr^{db}/J$ (*db/db*) mice (The Jackson Laboratory, Bar Harbor, ME) aged 20 weeks were used. Age-matched heterozygotes mice (*db/m*), a nonpenetrant genotype, were used as the control animals.

miRNA Drugs and Delivery

miRNA mimic and antagomiR oligonucleotides are highly stable and have been successfully used in vitro and in vivo to effectively elevate or silence endogenous miRNA (20,21). The properties of chemically engineered miRNA mimics (GE Dharmacon, Lafayette, CO) used in the experiment comprise a double-stranded construct consisting of guide and passenger strands, as previously described (20,22). To enable highly efficient delivery, double-strand miRNA mimics were formulated with a novel and nontoxic neutral lipid emulsion system (MaxSuppressor In Vivo RNA-Lancer II; BIOO Scientific, Austin, TX), as described in the vendor's manual. We delivered chemically modified miR-146a mimic oligos (catalog number MIMAT0000158; 5 or 10 mg/kg) to nondiabetic and diabetic mice via a tail vein using a syringe needle (27-gauge) under anesthesia with isoflurane. Treatments were performed once a week for a total of four injections.

Cel–miR-67 mimics were used as a negative control, which has been confirmed to have minimal sequence identity with miRNAs in human, mouse, and rat as well as have no identifiable effects on tested miRNA function (http://dharmacon.gelifesciences.com/microrna/miridian-microrna-mimic-negative-control-1/). The animals were sacrificed 4 weeks after last administration of miRNA under ketamine and xylazine anesthesia.

Measurement of Thermal Sensitivity

To examine the sensitivity to noxious heat, plantar and tail flick tests were measured using a thermal stimulation meter (IITC model 336 TG; IITC Life Science, Woodland Hills, CA) (23,24). For plantar test, the meter was activated after placing the stimulator directly beneath the plantar surface of the hind paw. The paw-withdrawal latency in response to the radiant heat (15% intensity and cutoff time 30 s) was recorded. For tail-flick test, the meter was set at 40% heating intensity with a cutoff at 10 s. For both tests, at least five readings per animal were taken at 15-min intervals, and the average was calculated (23,24).

Tactile Allodynia Test

Von Frey filaments were used to stimulate paw withdrawal. Briefly, a series of filaments were applied to the plantar surface of the left hind paw with a pressure, causing the filament to buckle. A paw withdrawal in response to each stimulus was recorded, and a 50% paw withdrawal threshold was calculated according to a published formula (24,25).

Electrophysiology Measurements

Sciatic nerve conduction velocity was assessed with orthodromic recording techniques, as previously described (23,24). During the measurements, animal rectal temperature was kept at 37°C using a feedback-controlled water bath. Motor nerve conduction velocity (MCV) and sensory nerve conduction velocity (SCV) were calculated according to our published studies (23,24).

Measurement of Regional Blood Flow and Plasma-Perfused Blood Vessels

Regional sciatic nerve blood flow was measured using a laser Doppler flowmetry (LDF; PeriFlux PF4; Perimed AB, Datavägen Sweden), as previously described (24). Relative flow values expressed as perfusion units were recorded under anesthesia. Regional sciatic nerve blood flow values from *db/m* mice were used as baseline values, and data are presented as a perfusion ratio.

To further examine blood perfusion in footpads and sciatic nerves, we used a laser Doppler perfusion imager system and analyzed with PIMSoft Software (Perimed AB). Mice were anesthetized, and the sensor was placed 10 cm above the footpad or exposed sciatic nerve. The apparatus displayed blood perfusion signal as a color-coded image ranging from dark blue (low perfusion) to bright red (high perfusion). To analyze the regional blood flow, we took time periods of interest and got the average regions of interest for each animal.

Fluorescein isothiocyanate (FITC)–dextran (2×10^6 molecular weight, 0.2 mL of 50 mg/mL; Sigma-Aldrich, St. Louis, MO) was intravenously injected to perfuse blood vessels (24,26). The density of FITC-dextran–perfused vessels was measured and divided by the total tissue area (mm^2) to determine vascular density.

Glucose, Glycosylated Hemoglobin, and Insulin Tolerance Tests

Plasma glucose was measured using a glucose meter (Ascensia Contour; Bayer, Zurich, Switzerland) once a week, and glycosylated hemoglobin (HbA_{1c}) levels (Quickmedical, Issaquah, WA) were measured every 2 weeks. For intraperitoneal

insulin tolerance test in the postabsorptive state, mice were fed and then fasted for 5 h. Either glucose (2 g/kg body weight) or human normal insulin (0.75 units/kg body weight) was injected intraperitoneally, and blood was collected from the tail vein at different time points.

Isolation of Spleen Cells and Peripheral Blood Mononuclear Cells

The spleens were removed and pressed through a nylon cell strainer (BD Falcon, Tewksbury, MA). The effluent samples were further filtered, suspended in red blood cell lysis buffer (eBioscience, San Diego, CA), and centrifuged. The splenocytes were checked for viability and used for Western blot or real-time RT-PCR analyses. Peripheral blood mononuclear cells (monocytes) were isolated with a Ficoll-Paque PLUS gradient (GE Healthcare, Pittsburgh, PA).

Fluorescence-Activated Cell Sorting

To isolate single-cell suspensions, an enzyme mix (MACS; Miltenyi Biotec, Auburn, CA) was added to the spleen tissue pieces. The tissues were filtered through a 70-μm cell strainer and resuspended in red blood cell lysis buffer. Then the pellets were resuspended in 100 μL flow cytometry staining buffer. Single splenocytes were stained with anti-mouse F4/80-allophycocyanin (APC) monoclonal antibody (Thermo Fisher Scientific, Waltham, MA) and anti-mouse CD11b-PE monoclonal antibody. The labeled cells were sorted on an SH800 flow cytometer (Sony Biotechnology, San Jose, CA).

Real-time Quantitative RT-PCR

Total RNAs from tissues or cells were isolated using the miRNeasy Kit (Qiagen, Germantown, MD), followed by reverse transcription and real-time quantitative RT-PCR as described in our previous publication (27). Relative quantities of miRNAs were calculated using the $2^{-\Delta\Delta Ct}$ method (28) with U6 snRNA (Applied Biosystems) as the endogenous control. RNAs from sera were isolated with miRNeasy Serum/Plasma Kit in conjunction with the synthetic spike-in control (cel–miR-39 mimic; Qiagen) for internal normalization. Quantitative detection of mRNA transcripts was carried out by real-time PCR with SYBR Green PCR mix (Applied Biosystems). Results were normalized to mRNA levels of β-actin. The primers used are given in Supplementary Tables 1 and 2.

miR-146a Target PCR Array

The mouse miR-146a Targets PCR Array (Qiagen) profiled the expression of 84 mmu–miR-146a-5p target genes. The protocol was conducted according to the vendor's manual. The expression of mRNAs was normalized against the expression of housekeeping genes from the array as an endogenous normalization control. Fold regulation changes for each mRNA were calculated by plugging the obtained threshold cycle values from PCR array data into manufacturer's Web-based software. The fold regulation is the negative inverse of the fold change ($-1/[2^{-\Delta\Delta Ct}]$) and indicates the changes of miR-146a target genes relative to control samples (*db/db* + miR con). Fold-regulation values less than one value indicate a negative or downregulation.

Bioinformatics Analysis

The TargetScan software (www.targetscan.org), an online miRNA target prediction algorithm, was used to predict the binding sequences of miR-146a target genes.

Immunohistochemistry and Image Analysis

The sciatic nerve and epidermal footpad tissues were used for immunohistochemistry. Semithin sections (2 μm) stained with toluidine blue were used to analyze myelin thickness (29). Morphometric analyses were performed using an MCID imaging system (Imaging Research Inc., St. Catharines, Ontario, Canada) according to our published protocols (23,24).

To measure intraepidermal nerve fibers (IENFs), the antibody against protein gene product 9.5 (PGP9.5, 1:1,000; Millipore) was applied on footpad tissue sections (23,24). IENF profiles were imaged under a ×40 objective (Carl Zeiss, Gottingen, Germany) via the MCID system. The number of nerve fibers crossing the dermal–epidermal junction were counted, and the density of nerves was expressed as fibers per millimeter length of section (23,24). Representative images of IENFs were obtained using a laser-scanning confocal microscope (Olympus FV2000; Olympus, Tokyo Japan).

Western Blotting and ELISA

Western blotting was performed as previously described (27), and antibodies used for these experiments are provided in Supplementary Table 3. ELISA (Thermo Fisher Scientific) was performed to quantify TNF-α and IL-1β concentrations in the sera.

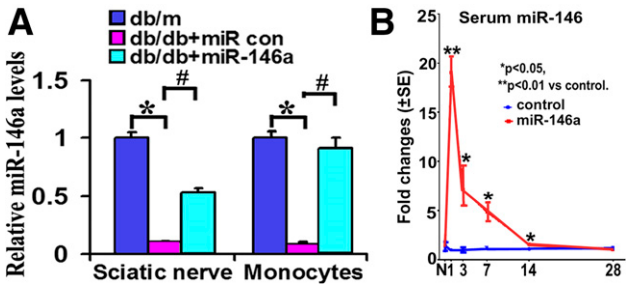

Figure 1—Levels of miR-146a expression. *A*: Quantitative real-time RT-PCR data show levels of miR-146a were decreased in sciatic nerves and monocytes of diabetic mice compared with tissues of nondiabetic mice. Nevertheless, *db/db* mice display significant elevation of miR-146a levels after treatment with miR-146a mimics. *B* illustrates the time course of serum levels of miR-146a in nontreated *db/m* mice treated with a single dose of miR-146a mimics (10 mg/kg; red) compared with levels in *db/m* mice treated with cel–miR-67 mimics (blue). n = 3/time point. *P < 0.05 and **P < 0.01 vs. control *db/m* animals; #P < 0.05 vs. *db/db* + miR con. con, control; N, normal.

Statistical Analysis

The data are presented as mean ± SE. Independent sample *t* test was used for two-group comparisons. One-way ANOVA followed by the Student-Newman-Keuls test were performed for multiple sample analysis. A value of $P < 0.05$ was taken as significant.

RESULTS

Treatment of Diabetic Mice With miR-146a Mimics Improves Neurological Function

Quantitative RT-PCR analysis revealed that *db/db* mice at the age of 20 weeks exhibited ~90% reduction of miR-146a levels in the sciatic nerve tissue and in monocytes compared with *db/m* mice (Fig. 1*A*). To investigate the effect of exogenous miR-146a on DPN, we first determined longitudinal serum levels of miR-146a after administration of miR-146a mimics, because stability is one of the main challenges for in vivo delivery of miRNA mimics, although chemically engineered miRNAs have been modified to reduce their degradation (20,21). A single dose of miR-146a mimics (10 mg/kg body weight) was intravenously administered to nondiabetic *db/m* mice via a tail vein, and sera were collected 1, 3, 7, 14, and 28 days after administration of miR-146a mimics ($n = 3$/time point). This dose of miR-146a mimics was based on studies published by others (28). Quantitative RT-PCR analysis showed that compared with cel–miR-67 mimics, the miR-146a mimic treatment significantly elevated miR-146a levels in sera over 14 days, with the highest elevation 1 day after the treatment (Fig. 1*B*). These data indicate that a single administration of miR-146a mimics elevates serum levels of miR-146a for 14 days in nondiabetic mice.

We then examined whether administration of miR-146a mimics affects miR-146a levels in the sciatic nerve tissue and monocytes of diabetic animals. The *db/db* mice at age of 20 weeks were treated weekly with miR-146a mimics (10 mg/kg) for 4 consecutive weeks, and sciatic nerve tissues and monocytes in blood were collected 24 h after the last treatment. Quantitative RT-PCR analysis showed that treatment with miR-146a mimics robustly elevated miR-146a levels in the sciatic nerve tissue and monocytes compared with cel–miR-67 mimics (Fig. 1*A*). Collectively, these data demonstrated that administration of miR-146a elevates miR-146a levels in blood and sciatic nerve tissue in nondiabetic and diabetic mice.

Next, we examined the effect of exogenous miR-146a on DPN (Fig. 2*A*). Compared with age-matched *db/m* mice,

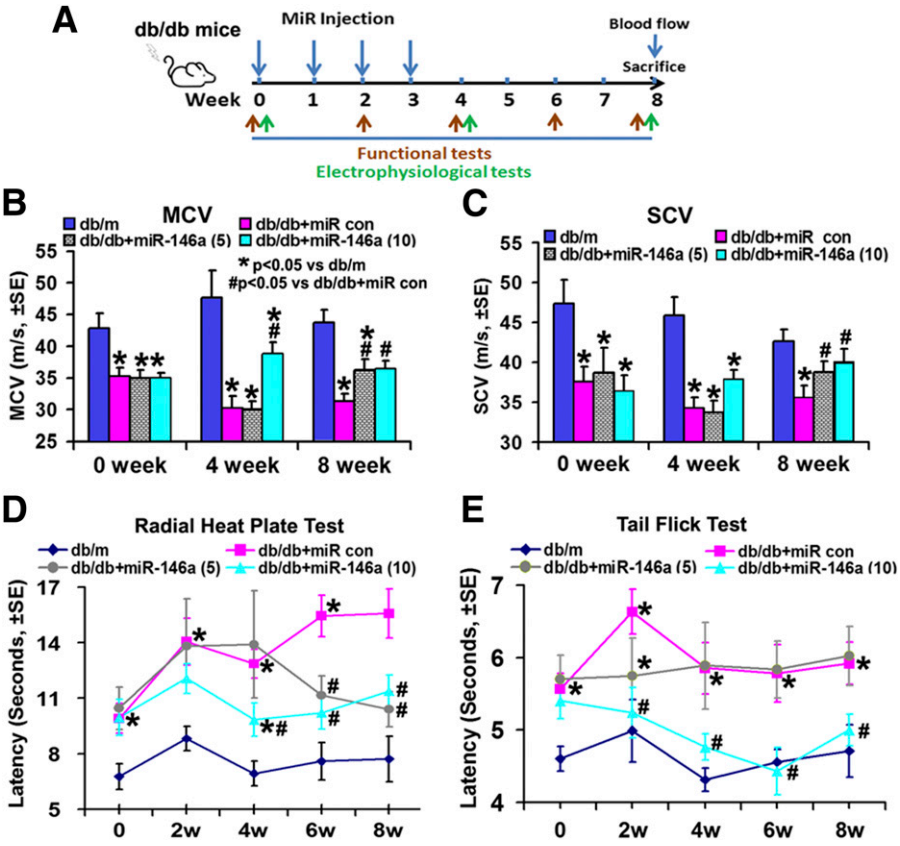

Figure 2—miR-146a treatment improves neurological function. *A*: Schematic diagram shows the treatment regimen of male *db/db* mice. Green arrows indicate time points of electrophysiological tests, and red arrows indicate time points of behavioral tests. Improved neurological function measured by MCV (*B*), SCV (*C*), radial heat plate test (*D*), and tail flick test (*E*) in *db/db* mice treated with miR-146a mimics (*db/db* + miR-146a, 5 and 10 mg/kg; $n = 13$/group) are shown. *$P < 0.05$ vs. nondiabetic mice (*db/m*; $n = 10$); #$P < 0.05$ vs. diabetic mice treated with control (con) miRNA mimics (*db/db* + miR con; $n = 13$). w, weeks.

db/db mice at age 20 weeks exhibited a significant reduction of MCV and SCV (Fig. 2*B* and *C*) ($P < 0.05$) and an increase in thermal response latencies measured by tail flick test and radial heat plate test (Fig. 2*D* and *E*), indicating that *db/db* mice at this age have DPN. Thus, *db/db* mice at age of 20 weeks were treated with miR-146a mimics at a dose of 5 or 10 mg/kg (body weight) once a week for 4 consecutive weeks. *db/db* mice that received cel–miR-67 mimics were used as a control group, as rodents do not express cel–miR-67 (30). Age-matched *db/m* mice were used as additional control groups. Animals were randomly assigned to control/treatment groups. All mice were sacrificed 4 weeks after termination of the last treatment (Fig. 2*A*). The duration of the experiment was 8 weeks. Compared with cel–miR-67 mimic control, miR-146a mimics at a dose of 10 mg/kg significantly improved MCV and SCV at 4 and 8 weeks, whereas a significant improvement was only detected 8 weeks after the initial treatment for miR-146a mimics at a dose of 5 mg/kg (Fig. 2*B* and *C*). Moreover, miR-146a at 10 mg/kg significantly reduced thermal response latencies measured by tail flick test and radial heat plate test, whereas 5 mg/kg miR-146a did not significantly alter thermal response latencies assayed by the tail flick test (Fig. 2*D* and *E*). These data indicate that miR-146a mimics at 10 mg/kg improve neurological outcomes of DPN. Thus, we analyzed the therapeutic mechanism based on the dose of 10 mg/kg miR-146a mimics.

miR-146a Treatment Improves Vascular Function in the Peripheral Nerve Tissues of Diabetic Mice

The treatment of *db/db* mice with miR-146a mimics did not significantly alter levels of blood glucose, HbA_{1c}, and insulin resistance compared with cel–miR-67 mimics at 8 weeks (Fig. 3*A–C*), indicating that the therapeutic effect of exogenous miR-146a on DPN is not induced by reducing glucose levels. In addition, the administration of miR-146a mimics did not significantly alter the animal body weight in *db/db* mice compared with diabetic mice treated with cel–miR-67 mimics, although a significant weight gain was detected in *db/db* mice compared with *db/m* mice (Fig. 3*D*).

Regional blood flow of sciatic nerve and footpad tissues has not been extensively studied in diabetic mice. We found that *db/db* mice at age of 20 weeks exhibited a significant reduction of blood flow in these two tissues measured with LDF compared with age-matched *db/m* mice (Supplementary Fig. 1*A* and *B*). The blood flow was further significantly decreased in *db/db* mice at the age of 28 weeks compared with 20-week-old mice (Supplementary Fig. 1*A* and *B*). These data suggest that diabetes induces progressive reduction of peripheral tissue perfusion. However, treatment of *db/db* mice with miR-146a mimics initiated at age of 20 weeks significantly increased the regional blood flow in the sciatic nerve tissue and footpads at age of 28 weeks compared with the miR-67 mimic treatment (Fig. 4*A–C*).

To examine whether increased regional blood flow by miR-146a mimics is related to augmentation of blood vessels, we intravenously injected FITC-dextran and permitted FITC-dextran to circulate within blood for 5 min prior to sacrifice. Thus, FITC-dextran within blood circulates within all functional blood vessels (31). We found that miR-146a mimics significantly increased FITC-dextran–perfused blood vessels in the sciatic nerve tissue compared with the cel–miR-67 mimics (Fig. 4*D* and *E*). Together with LDF

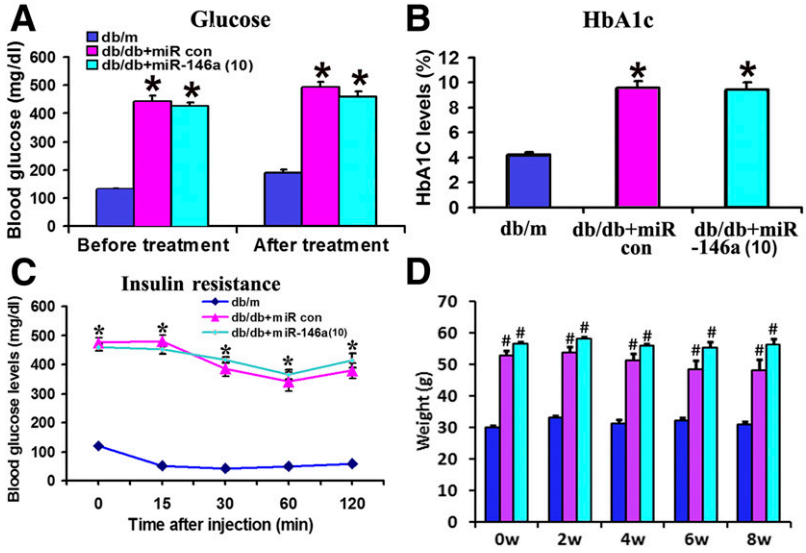

Figure 3—Effect of miR-146a treatment on glucose levels, insulin sensitivity, and weight gain. Levels of blood glucose (*A*), HbA_{1c} (*B*), and insulin resistance (*C*) were not altered in *db/m* and *db/db* mice 8 weeks after the initial treatment with miR-146a mimics or cel–miR-67 mimics (10 mg/kg). *C* shows insulin tolerance test lasting for 2 h. The test was conducted with insulin at 1.0 units/kg body weight (intraperitoneally). *D* shows the effect of miR-146 treatment on animal weight gain. n = 10/group. *$P < 0.05$ and #$P < 0.01$ vs. *db/m*. con, control; w, weeks.

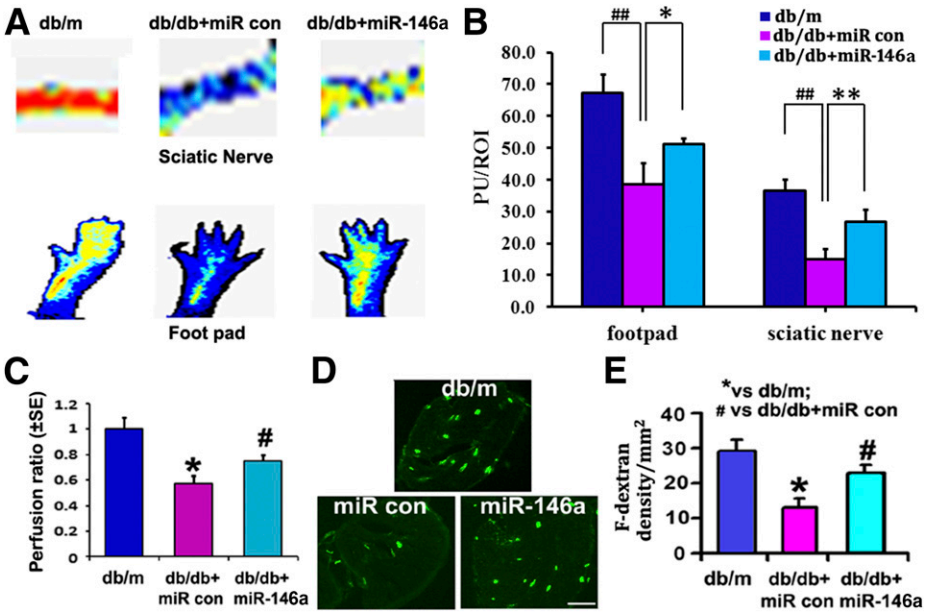

Figure 4—miR-146a treatment improves neurovascular function. *A* shows representative images of regional blood flow in footpad and sciatic nerve tissues 8 weeks after miR-146a mimic treatment. *B* shows the quantitative analysis of blood flow based on laser Doppler perfusion imaging. Diabetic miR-146a injection markedly increased perfusion of sciatic nerve and footpad in diabetic mice. Lowest blood flow is indicated in blue, maximum blood flow in red, and intermediate grading in green and yellow. *C* shows the perfusion ratio of blood flow normalized with *db/m* mice in sciatic nerves. Images of FITC-dextran (F-dextran) perfused vessels (*D*) and the quantitative data of perfused vascular area (*E*), respectively, in *db/m* mice and *db/db* mice treated with miR-146a mimics (10 mg/kg, *db/db* + miR-146a) or cel–miR-67 mimics (*db/db* + miR control [con]). n = 4/group in *C*. n = 10 for *db/m* group; n = 13 for *db/db* + miR con and *db/db* + miR-146a groups in *A*, *D*, and *E*. Scale bar = 100 μm. $^*P < 0.05$ and $^{**}P < 0.01$ vs. nondiabetic (*db/m*) mice; $\#P < 0.05$ and $\#\#P < 0.01$ vs. *db/db* mice treated with cel–miR-67 mimics (*db/db* + miR con). PU, perfusion units; ROI, region of interest.

data, these results indicate that miR-146a mimics improve peripheral tissue perfusion.

miR-146a Treatment Improves Nerve Function

IENFs innervate dermis and epidermis, and a measurement of IENF density through skin biopsy has been widely used in the clinical diagnosis of peripheral neuropathy and in monitoring its response to treatment (32). We analyzed the IENF densities of the footpads and found that the number of PGP9.5-positive IENFs in *db/db* mice at age of 20 and 28 weeks was significantly reduced compared with that in age-matched *db/m* mice (Supplementary Fig. 2). Moreover, *db/db* mice had significantly lower IENF densities at the age of 28 weeks than at 20 weeks (Supplementary Fig. 2). In contrast, miR-146a mimic treatment almost completely suppressed diabetes-induced reduction of IENFs compared with the cel–miR-67 mimics in *db/db* mice aged 28 weeks (Fig. 5).

miR-146a Treatment Increases Axonal Myelination

Microvasculature dysfunction accompanies demyelination and severe loss of myelinated axons in peripheral nerves, which are related to the progression of DPN (2). To examine the effect of miR-146 mimics on myelination and axons, we measured myelinated sciatic nerves on semithin transverse sections stained with toluidine blue (29). Myelinated fiber diameter and myelin sheath thickness were measured using MCID image analysis software, and g-ratio was calculated to determine the degree of myelination (23). We found a significant reduction of myelin thickness and fiber diameter in *db/db* mice aged 20 weeks, which were further reduced at 28 weeks of age compared with age-matched *db/m* mice (Supplementary Fig. 3 and Supplementary Table 4). Treatment of *db/db*

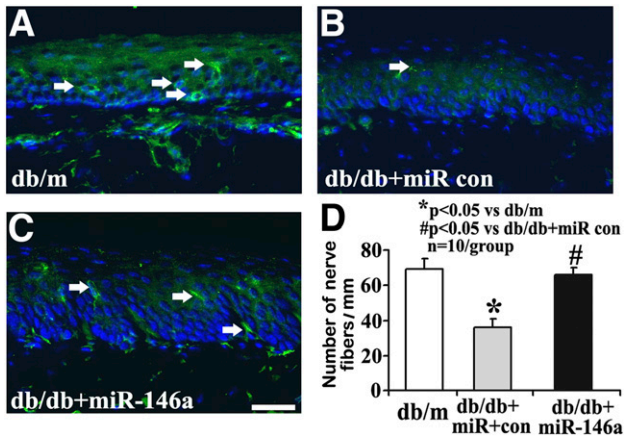

Figure 5—miR-146a treatment inhibits diabetes-induced loss of IENF. Representative immunofluorescent images show PGP9.5 staining IENF (green, arrows) and epidermal innervation in the hind plantar paw skin of *db/m* mice (*A*) and diabetic mice treated with cel–miR-67 mimics (*db/db* + miR control [con]; *B*). The increase of PGP9.5-positive nerve fibers is evident following miR-146a mimics (10 mg/kg, *db/db* + miR-146a; *C*). Histogram represents the mean number of IENF per site under various treated conditions (*D*). n = 10/group. Scale bar = 50 μm. $^*P < 0.05$ compared with *db/m* group; $\#P < 0.05$ compared with *db/db* + miR con group.

mice with miR-146a mimics significantly increased myelin thickness and considerably reduced g-ratio compared with control miRNA mimics at the age of 28 weeks (Fig. 6).

miR-146a Treatment Regulates IRAK1/TRAF6 and Their Downstream Proinflammatory Gene Expression

miRNAs control gene expression through regulating its target gene translation and/or stability (33). Using a new miR-146a target PCR array, which includes 84 currently known experimentally verified plus bioinformatically predicted target genes regulated by miR-146a, we screened the target genes in peripheral tissues. Administration of miR-146a mimics to diabetic mice robustly downregulated a number of target mRNAs, including IRAK1/2 and TRAF6 in the sciatic nerves and monocytes (Fig. 7*A–C*). Using quantitative real-time RT-PCR and Western blot, we validated mRNA (Fig. 7*D* and *E*) and protein levels (Fig. 7*F*) of target genes including IRAK1, TRAF6, and ADAMTS3, respectively, in the sciatic nerves and monocytes of *db/db* mice. IRAK1/TRAF6 genes have been experimentally confirmed as miR-146a target genes (13), and ADAMTS3 is a bioinformatically predicted miR-146a target gene (Fig. 7*C*) that plays an important role in inflammation (34). *db/db* mice treated with cel–miR-67 mimics exhibited substantial elevation of IRAK1, TRAF6, and ADAMTS3 mRNAs in sciatic nerves (Fig. 7*D*) and monocytes (Fig. 7*E*) as well as proteins within sciatic nerves (Fig. 7*F*), compared with nondiabetic *db/m* mice. However, miR-146a mimics robustly suppressed the expression of these genes compared with cel–miR-67 mimics (Fig. 7*D–F*). Moreover, miR-146a mimics also reduced the component of nuclear factor-κB (NF-κB) signaling, including p65, in the sciatic nerve augmented by diabetes (Fig. 7*F*).

miR-146a Treatment Alters the Macrophage Phenotype and Reduces Inflammatory Responses

Recent studies from patients with diabetes showed that diabetes increased classically activated (M1) phenotype macrophages (35). To elucidate the relationship between miR-146a and macrophage inflammation in vivo, we measured expression of key genes that have been used as markers of M1 (proinflammatory) macrophages or alternatively activated (M2; anti-inflammatory) macrophages in mouse spleen tissues (Fig. 8*A* and *B*) and splenic macrophages (Fig. 8*C* and *D*). Lineage F4/80$^+$CD11b$^+$ macrophages were purified with FACS from single spleen cell suspensions that were labeled with antibodies against macrophage markers (F4/80 and CD11b) (Fig. 8*C*). Western blot (Fig. 8*A* and *B*) and quantitative RT-PCR data (Fig. 8*D*) showed that compared with nondiabetic *db/m* mice, diabetic *db/db* mice exhibited a significant increase in mRNA levels of proinflammatory M1 marker genes TNF-α, IL-1β, and inducible nitric oxide synthase (iNOS) but substantial reduction of the anti-inflammatory M2 marker gene Ym1 in splenic macrophages. Conversely, miR-146a mimics completely reversed diabetes-increased M1 marker and -reduced M2 marker transcripts compared with cel–miR-67 mimics (Fig. 8*A*, *B*, and *D*), suggesting that miR-146a alters macrophage inflammatory polarization. In addition, we found that miR-146a mimics significantly reduced diabetes-augmented serum levels of TNF-α and IL-1β, as measured with ELISA (Fig. 8*E* and *F*).

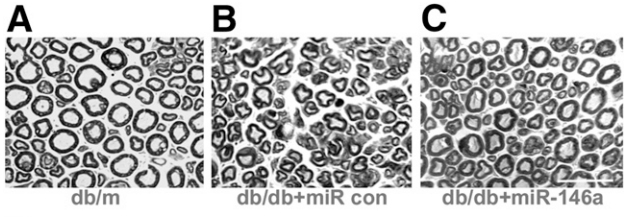

D Effect of miR-146a mimics on histomorphometric parameter of sciatic nerves

Property	db/m	db/db+miR con	db/db+miR-146a
Axon diameter(μm)	5.18±0.14**	4.70±0.08	5.18±0.09**
Fiber diameter(μm)	8.66±0.17***	7.54±0.14	8.70±0.16***
myelin thickness(μm)	1.74±0.06***	1.42±0.03	1.75±0.05***
g ratio	0.59±0.01*	0.62±0.005	0.59±0.006**

Values are mean±SE. *P<0.05, **P<0.01, ***P<0.001 vs db/db+miR con

Figure 6—Effect of miR-146a treatment on morphometric changes of myelinated sciatic nerves. Representative images of semithin toluidine blue–stained transverse sections of sciatic nerves derived from nondiabetic mice (*db/m*; *A*), diabetic mice treated with cel–miR-67 mimics (*db/db* + miR control [con]; *B*), or diabetic mice treated with miR-146a (10 mg/kg, *db/db* + miR-146a; *C*). The quantitative data of histomorphometric parameters of sciatic nerves (*D*) show that mean fiber and axon diameters as well as myelin sheath thickness were reduced in diabetic mice treated with cel–miR-67 mimics, but nevertheless increased in miR-146a–treated diabetic mice. Mean g-ratio was significantly increased in diabetic animals, indicating mild hypomyelination and miR-146a treatment leads to a significant reduction of myelinated fiber density. n = 10/group. Scale bar = 25 μm. *P < 0.05, **P < 0.01, and ***P < 0.001 vs. diabetic mice treated with cel–miR-67 mimics (*db/db* + miR con).

DISCUSSION

In a novel set of experiments, our data show that intravenous administration of miR-146a mimics remarkably improved sciatic nerve vascular function, axonal myelination, and peripheral nerve function in diabetic mice, suggesting that exogenous miR-146a may have a therapeutic effect on the clinical treatment of DPN.

The current study demonstrates that treatment of diabetic mice with miR-146a mimics substantially improves peripheral nerve tissue perfusion, which is closely associated with increased IENF density and myelination. These findings suggest that improved neurovascular functions by miR-146 mimics likely lead to ameliorating DPN. Microvasculature dysfunction accompanies demyelination, and severe loss of myelinated axons in peripheral nerves and microvascular damage either precedes or parallels the impairment of nerve function as DPN progresses (2,3,36). In parallel, our data demonstrated that *db/db* mice at the age of 20 weeks exhibited neurovascular dysfunction that was associated with DPN and that impaired neurovascular function further progressed during 20 to 28 weeks. Moreover, treatment with miR-146a mimics initiated at age of 20 weeks prevented

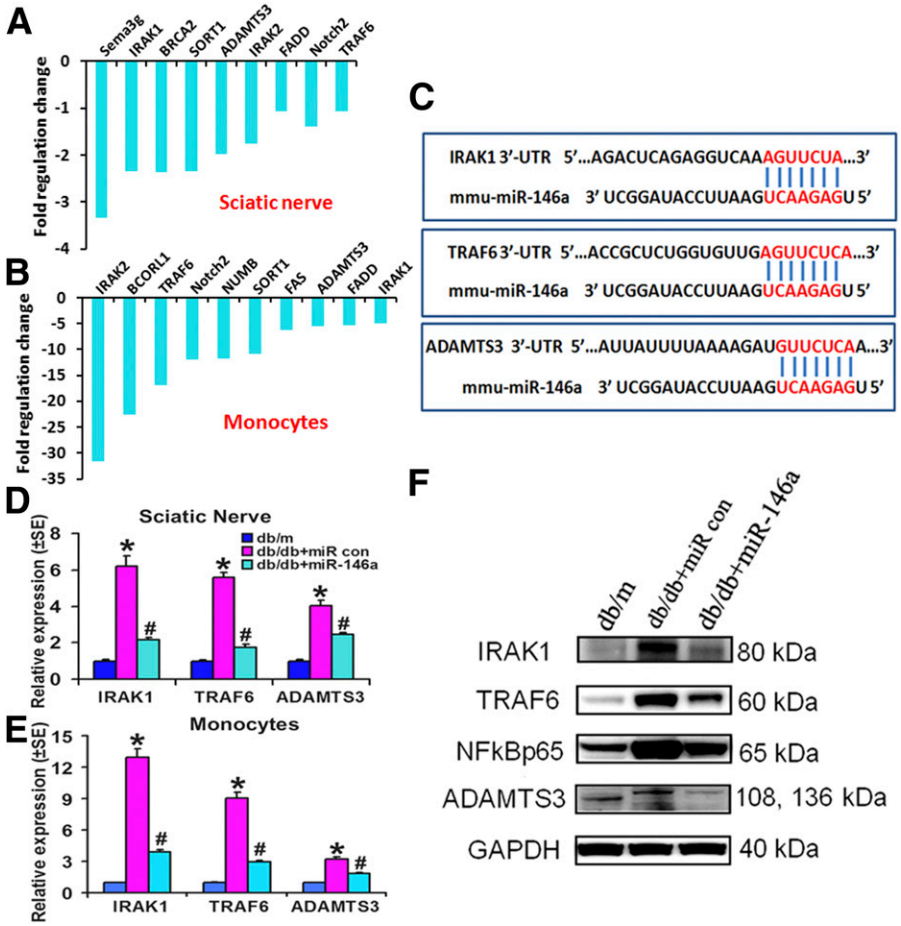

Figure 7—miR-146a treatment reduces inflammatory response via regulating target gene expression. miR-146a target PCR array shows highly differentially downregulated putative target genes of miR-146a in the sciatic nerves (*A*) and monocytes (*B*) in *db/db* mice treated with miR-146a or control (con) miRNA mimics. In silico TargetScan-predicted complementarity between miR-146a and 3′-untranslated regions (UTR) of predicted target genes including IRAK1, TRAF6, and ADAMTS3 is shown in *C*. Real-time RT-PCR validated the downregulated putative target genes of miR-146a detected by miR-146a target PCR array in the sciatic nerves (*D*) and monocytes (*E*) isolated from *db/db* mice treated with miR-146a or control cel–miR-67 mimics (10 mg/kg) at 24 h after the last treatment. *F*: Western blot analysis of target genes IRAK1 and TRAF6 and downstream NF-κB signaling as well as a new potential target gene, ADAMTS3, of miR-146a (10 mg/kg) in sciatic nerves harvested from *db/db* mice treated with miR-146a mimics or cel–miR-67 mimics and from nondiabetic mice (*db/m*) at 24 h after the last treatment. *$P < 0.05$ and #$P < 0.05$ compared with diabetic *db/db* mice treated with control cel–miR-67.

further impairment of the neurovascular function, but did not reverse neurovascular damage induced by diabetes prior to the treatment. Although the current study does not provide the cause–effect of vasculature on nerve fiber and axonal damage, our results suggest that they are highly correlated, implying that restoring blood flow to the vasa nervorum contributes to the improvement of nerve function in experimental DPN model. We previously demonstrated that sildenafil treatment initiated at an early stage of DPN achieves more robust therapeutic effect than when the treatment was administered to middle-aged diabetic *db/db* mice with advanced peripheral neuropathy (31). The present findings suggest that the miR-146a mimic treatment initiated at an early stage of DPN may maximize the therapeutic effect of miR-146a mimics.

The current study shows that administration of miR-146a mimics does not significantly reduce blood levels of glucose, HbA_{1c}, and animal body weight, suggesting the therapeutic action is not via reducing glucose levels. Downregulation of miR-146a is related to the activation of the NF-κB signaling pathway in diabetic animals and patients with diabetes (8,10,37–40). Our miRNA target PCR array revealed that miR-146a mimics greatly suppressed expression of many proinflammatory genes, including IRAK1, TRAF6, and ADAMTS3, which are target genes of miR-146a. IRAK1 and TRAF6 are downstream adaptors of Toll-like receptors (TLRs), a family of pattern-recognition receptors responsible for the initiation of inflammatory and immune responses. TLR2 and TLR4 are involved in the perpetuation of inflammation during diabetic neuropathy (39,40). The deregulation of TLRs in DPN can activate their subsequent IRAK1, TRAF6, and downstream NF-κB, which results in the synthesis and secretion of cytokines and chemokines (39,40).

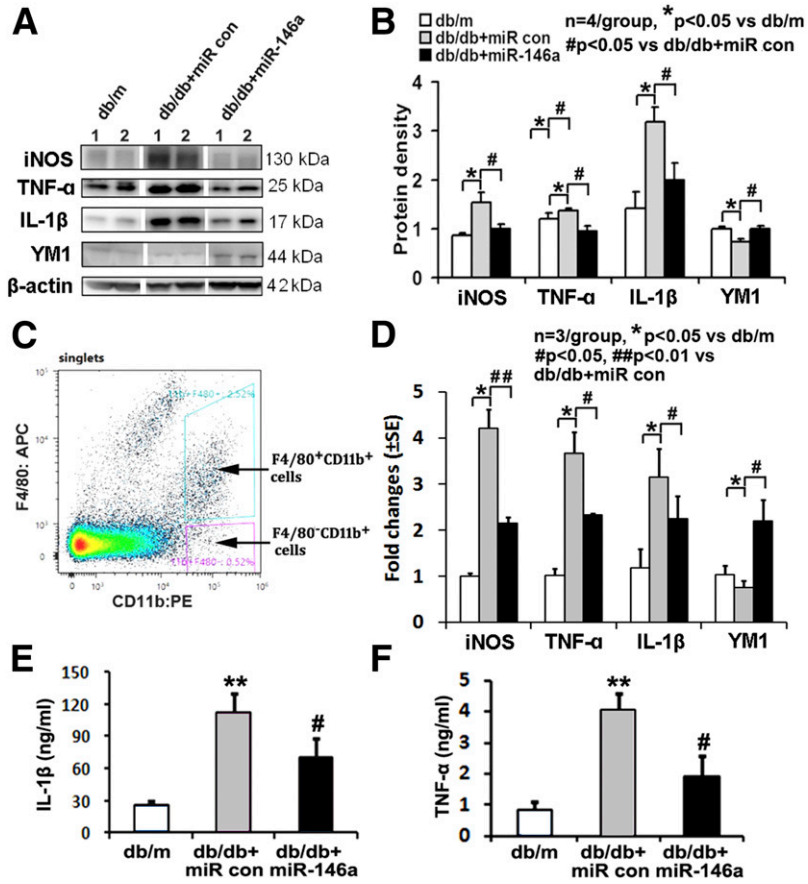

Figure 8—miR-146a regulates macrophage polarization. Representative Western blots (*A*) and their quantitative data (*B*) show protein levels of proinflammatory M1 markers TNF-α, iNOS, and IL-1β were significantly increased, but anti-inflammatory M2 marker YM1 was decreased in splenic tissues isolated from diabetic *db/db* mice. However, treatment of diabetic *db/db* mice with miR-146a mimics completely reversed diabetes-increased M1 marker proteins and -reduced M2 marker protein compared with cel–miR-67 mimic treatment. *C*: Whole spleen cell suspensions were labeled with antibodies against macrophage lineage markers (F4/80 and CD11b), and lineage $F4/80^{+}CD11b^{+}$ cells were sorted by FACS. Dot plots correspond to a representative staining in the splenocytes with gates used for sorting. *D*: Total RNAs from sorted splenic macrophages were analyzed by real-time RT-PCR for TNF-α, iNOS, IL-1β, and YM1; values are relative to expression of the gene encoding β-actin. The miR-146a treatment reduces serum IL-1β (*E*) and TNF-α (*F*) concentrations analyzed via ELISA in diabetic mice compared with mice treated with control (con) miR. $^{*}P < 0.05$ and $^{**}P < 0.01$ compared with nondiabetic *db/m* mice; $\#P < 0.05$ and $\#\#P < 0.01$ compared with diabetic *db/db* mice treated with control cel–miR-67.

We previously demonstrated that fibrin downregulated miR-146a and upregulated IRAK1 and that elevation of miR-146a repressed IRAK1, which results in attenuation of NF-κB activation, consequently leading to diminished inflammatory responses in human brain endothelial cells (41). Hyperglycemia in patients with diabetes triggers thrombosis, and activation of NF-κB plays a key role in hyperglycemia-induced neurovascular dysfunction (42,43). Thus, our data suggest that miR-146 mimics suppress NF-κB signaling-activated inflammation via its target genes, IRAK and TRAF6, and consequently reduce thrombosis, leading to improved peripheral tissue perfusion. Others have shown that miR-146a increases angiogenesis in human umbilical vein endothelial cells (44). Thus, the effects of miR-146a on vascularization in sciatic nerves of diabetic mice warrant further study.

We previously demonstrated that miR-146a via TLR signaling regulates dorsal root ganglion neuron axonal outgrowth and apoptosis under hyperglycemia conditions (45). Moreover, miR-146a promotes oligodendrocyte progenitor cells to differentiate into myelinating oligodendrocytes (27). These data suggest that in addition to its role in vascular function, miR-146a mimics could directly act on distal axons of dorsal root ganglion neurons and Schwann cells and contribute to increased nerve fibers and myelination. Thus, additional studies are warranted for further investigating these effects in DPN.

In conclusion, elevation of miR-146a levels in mice with DPN reduces neurovascular dysfunction, which provides a permissive restorative and neurovascular remodeling and thereby ameliorates peripheral neuropathy.

Acknowledgments. The authors thank Julie Landschoot-Ward, Cindi Robert, and Qing-e Lu (Department of Neurology, Henry Ford Health System) for immunohistochemistry staining.

Funding. This work was supported by National Institutes of Health National Institute of Diabetes and Digestive and Kidney Diseases grant RO1-RDK-102861A (to X.S.L.), American Heart Association grant-in-aid 14GRNT20460167 (to X.S.L.), and National Institute of Neurological Disorders and Stroke grants RO1-NS-088656 (to M.C.) and RO1-NS-075156 (to Z.G.Z.).

Duality of Interest. X.S.L., L.W., M.C., and Z.G.Z. reported holding U.S. patent WO 2014113822 A1. No other potential conflicts of interest relevant to this article were reported.

Author Contributions. X.S.L. and Z.G.Z. designed the study. X.S.L., B.F., A.S., L.J., X.W., L.Z., and R.Z. conducted the animal experiments. X.S.L., B.F., A.S., L.W., W.P., J.H., and X.M.Z. analyzed and interpreted data. X.S.L., M.C., and Z.G.Z. wrote the manuscript. All authors approved the manuscript. X.S.L. and Z.G.Z. are the guarantors of this work and, as such, had full access to all of the data in the study and take responsibility for the integrity of the data and the accuracy of the data analysis.

References

1. Boucek P. Advanced diabetic neuropathy: a point of no return? Rev Diabet Stud 2006;3:143–150
2. Cameron NE, Eaton SE, Cotter MA, Tesfaye S. Vascular factors and metabolic interactions in the pathogenesis of diabetic neuropathy. Diabetologia 2001;44:1973–1988
3. Cameron NE, Cotter MA, Low PA. Nerve blood flow in early experimental diabetes in rats: relation to conduction deficits. Am J Physiol 1991;261:E1–E8
4. Cameron NE, Gibson TM, Nangle MR, Cotter MA. Inhibitors of advanced glycation end product formation and neurovascular dysfunction in experimental diabetes. Ann N Y Acad Sci 2005;1043:784–792
5. Kusano KF, Allendoerfer KL, Munger W, et al. Sonic hedgehog induces arteriogenesis in diabetic vasa nervorum and restores function in diabetic neuropathy. Arterioscler Thromb Vasc Biol 2004;24:2102–2107
6. Demiot C, Tartas M, Fromy B, Abraham P, Saumet JL, Sigaudo-Roussel D. Aldose reductase pathway inhibition improved vascular and C-fiber functions, allowing for pressure-induced vasodilation restoration during severe diabetic neuropathy. Diabetes 2006;55:1478–1483
7. Ii M, Nishimura H, Kusano KF, et al. Neuronal nitric oxide synthase mediates statin-induced restoration of vasa nervorum and reversal of diabetic neuropathy. Circulation 2005;112:93–102
8. Nguyen DV, Shaw LC, Grant MB. Inflammation in the pathogenesis of microvascular complications in diabetes. Front Endocrinol (Lausanne) 2012;3:170
9. Wilson NM, Wright DE. Inflammatory mediators in diabetic neuropathy. J Diabetes Metab 2011;S5:004
10. Duksal T, Tiftikcioglu BI, Bilgin S, Kose S, Zorlu Y. Role of inflammation in sensory neuropathy in prediabetes or diabetes. Acta Neurol Scand 2016;133:384–390
11. Yamakawa I, Kojima H, Terashima T, et al. Inactivation of TNF-α ameliorates diabetic neuropathy in mice. Am J Physiol Endocrinol Metab 2011;301:E844–E852
12. Zampetaki A, Mayr M. MicroRNAs in vascular and metabolic disease. Circ Res 2012;110:508–522
13. Li L, Chen XP, Li YJ. MicroRNA-146a and human disease. Scand J Immunol 2010;71:227–231
14. Xu J, Wu W, Zhang L, et al. The role of microRNA-146a in the pathogenesis of the diabetic wound-healing impairment: correction with mesenchymal stem cell treatment. Diabetes 2012;61:2906–2912
15. Kovacs B, Lumayag S, Cowan C, Xu S. MicroRNAs in early diabetic retinopathy in streptozotocin-induced diabetic rats. Invest Ophthalmol Vis Sci 2011;52:4402–4409
16. Kaidonis G, Gillies MC, Abhary S, et al. A single-nucleotide polymorphism in the MicroRNA-146a gene is associated with diabetic nephropathy and sight-threatening diabetic retinopathy in Caucasian patients. Acta Diabetol 2016;53:643–650
17. Li Y, Zhang Y, Li X, et al. Association study of polymorphisms in miRNAs with T2DM in Chinese population. Int J Med Sci 2015;12:875–880
18. Ciccacci C, Morganti R, Di Fusco D, et al. Common polymorphisms in MIR146a, MIR128a and MIR27a genes contribute to neuropathy susceptibility in type 2 diabetes. Acta Diabetol 2014;51:663–671
19. Sullivan KA, Hayes JM, Wiggin TD, et al. Mouse models of diabetic neuropathy. Neurobiol Dis 2007;28:276–285
20. van Rooij E, Sutherland LB, Thatcher JE, et al. Dysregulation of microRNAs after myocardial infarction reveals a role of miR-29 in cardiac fibrosis. Proc Natl Acad Sci U S A 2008;105:13027–13032
21. Bonauer A, Carmona G, Iwasaki M, et al. MicroRNA-92a controls angiogenesis and functional recovery of ischemic tissues in mice. Science 2009;324:1710–1713
22. van Rooij E, Kauppinen S. Development of microRNA therapeutics is coming of age. EMBO Mol Med 2014;6:851–864
23. Wang L, Chopp M, Szalad A, et al. Phosphodiesterase-5 is a therapeutic target for peripheral neuropathy in diabetic mice. Neuroscience 2011;193:399–410
24. Wang L, Chopp M, Szalad A, et al. Thymosin β4 promotes the recovery of peripheral neuropathy in type II diabetic mice. Neurobiol Dis 2012;48:546–555
25. Chaplan SR, Bach FW, Pogrel JW, Chung JM, Yaksh TL. Quantitative assessment of tactile allodynia in the rat paw. J Neurosci Methods 1994;53:55–63
26. Zhang Z, Davies K, Prostak J, Fenstermacher J, Chopp M. Quantitation of microvascular plasma perfusion and neuronal microtubule-associated protein in ischemic mouse brain by laser-scanning confocal microscopy. J Cereb Blood Flow Metab 1999;19:68–78
27. Liu XS, Chopp M, Pan WL, et al. MicroRNA-146a promotes oligodendrogenesis in stroke. Mol Neurobiol 2017;54:227–237
28. Livak KJ, Schmittgen TD. Analysis of relative gene expression data using real-time quantitative PCR and the 2(-Delta Delta C(T)) method. Methods 2001;25:402–408
29. Di Scipio F, Raimondo S, Tos P, Geuna S. A simple protocol for paraffin-embedded myelin sheath staining with osmium tetroxide for light microscope observation. Microsc Res Tech 2008;71:497–502
30. Katakowski M, Buller B, Wang X, Rogers T, Chopp M. Functional microRNA is transferred between glioma cells. Cancer Res 2010;70:8259–8263
31. Wang L, Chopp M, Szalad A, et al. Sildenafil ameliorates long term peripheral neuropathy in type II diabetic mice. PLoS One 2015;10:e0118134
32. Lauria G, Hsieh ST, Johansson O, et al. European Federation of Neurological Societies/Peripheral Nerve Society Guideline on the use of skin biopsy in the diagnosis of small fiber neuropathy. Report of a joint task force of the European Federation of Neurological Societies and the Peripheral Nerve Society. Eur J Neurol 2010;17:903–912
33. Fabian MR, Sonenberg N, Filipowicz W. Regulation of mRNA translation and stability by microRNAs. Annu Rev Biochem 2010;79:351–379
34. Lemarchant S, Pruvost M, Montaner J, et al. ADAMTS proteoglycanases in the physiological and pathological central nervous system. J Neuroinflammation 2013;10:133
35. Satoh N, Shimatsu A, Himeno A, et al. Unbalanced M1/M2 phenotype of peripheral blood monocytes in obese diabetic patients: effect of pioglitazone. Diabetes Care 2010;33:e7
36. Ebenezer GJ, O'Donnell R, Hauer P, Cimino NP, McArthur JC, Polydefkis M. Impaired neurovascular repair in subjects with diabetes following experimental intracutaneous axotomy. Brain 2011;134:1853–1863
37. Forbes JM, Cooper ME. Mechanisms of diabetic complications. Physiol Rev 2013;93:137–188
38. Pop-Busui R, Ang L, Holmes C, Gallagher K, Feldman EL. Inflammation as a therapeutic target for diabetic neuropathies. Curr Diab Rep 2016;16:29
39. Dasu MR, Devaraj S, Park S, Jialal I. Increased toll-like receptor (TLR) activation and TLR ligands in recently diagnosed type 2 diabetic subjects. Diabetes Care 2010;33:861–868
40. Dasu MR, Ramirez S, Isseroff RR. Toll-like receptors and diabetes: a therapeutic perspective. Clin Sci (Lond) 2012;122:203–214
41. Zhang L, Chopp M, Liu X, et al. Combination therapy with VELCADE and tissue plasminogen activator is neuroprotective in aged rats after stroke and targets microRNA-146a and the toll-like receptor signaling pathway. Arterioscler Thromb Vasc Biol 2012;32:1856–1864

42. Paneni F, Beckman JA, Creager MA, Cosentino F. Diabetes and vascular disease: pathophysiology, clinical consequences, and medical therapy: part I. Eur Heart J 2013;34:2436–2443
43. Creager MA, Lüscher TF, Cosentino F, Beckman JA. Diabetes and vascular disease: pathophysiology, clinical consequences, and medical therapy: Part I. Circulation 2003;108:1527–1532
44. Zhu HY, Bai WD, Liu JQ, et al. Up-regulation of FGFBP1 signaling contributes to miR-146a-induced angiogenesis in human umbilical vein endothelial cells. Sci Rep 2016;6:25272
45. Jia L, Wang L, Chopp M, Zhang Y, Szalad A, Zhang ZG. MicroRNA 146a locally mediates distal axonal growth of dorsal root ganglia neurons under high glucose and sildenafil conditions. Neuroscience 2016;329:43–53